Vector magnetometry based on $S = \frac{3}{2}$ electronic spins

Sang-Yun Lee,* Matthias Niethammer, and Jörg Wrachtrup
3rd Institute of Physics, University of Stuttgart, Pfaffenwaldring 57, 70569 Stuttgart, Germany
(Received 26 May 2015; revised manuscript received 12 August 2015; published 1 September 2015)

Electronic spin systems with S > 1/2 provide an efficient method for dc vector magnetometry, since the conventional electron spin resonance spectra at a given magnetic field reflect not only the field strength but also orientation in the presence of strong spin-spin interactions. $S = 1$ spins, e.g., the nitrogen-vacancy centers in diamond, have been intensively investigated for such a purpose. In this report, we compare $S = 1$ and 3/2 spins, and discuss how one can apply general principles for the use of high-spin systems as a vector magnetometer to the $S = 3/2$ spin systems. We find analytical solutions which allow a reconstruction of the magnetic field strength and polar angle using the observed resonance transitions if a uniaxial symmetry exists for the spin-spin interaction as in $S = 1$ systems. We also find that an ambiguity of determining the field parameters may arise due to the unique properties of $S = 3/2$ systems, and present solutions for it utilizing additional transitions in the low-field region. The electronic spins of the silicon vacancy in silicon carbide will be introduced as a model for the $S = 3/2$ dc vector magnetometer and the practical usage of it, including the magic-angle spinning type method, will be presented too.

DOI: 10.1103/PhysRevB.92.115201 PACS number(s): 76.20.+q, 76.30.−v, 76.70.Hb

I. INTRODUCTION

Electronic spins in highly localized defects, such as the nitrogen-vacancy (NV) centers in diamond [1,2] and vacancy related defects in silicon carbide (SiC) [3–14], may experience a strong spin-spin interaction, e.g., a dipole-dipole interaction, which results in the so-called zero-field splitting (ZFS), partially (or completely) lifting degeneracy of energy eigenstates at zero magnetic field [15,16]. If this interaction is strong enough, the eigenvalues of the spin Hamiltonian show a strong dependence on the orientation of the applied magnetic field. Such dependence causes a nonlinear shift of resonance transitions in electron spin resonance (ESR) spectra. Thus the information about the applied external magnetic field can be extracted from ESR spectra provided the ZFS is known.

One well-known example is the NV center in diamond. Its application to dc field vector magnetometry has been reported and well understood in the field strength from sub-micro-tesla to a few tenth tesla [17–20]. The NV center has a triplet ground state of $S = 1$ and when shifts of the ESR transition at a given dc magnetic field are directly monitored in the frequency domain, typically a ∼0.1 mT minimum detectable magnetic field is achieved [21]. This resolution is limited by the ESR linewidth, which can be broadened by strong RF fields thus lowering the resolution. Lower RF power can be used to avoid power broadening, but the decreased signal strength requires a very long accumulation time. If time-domain experiments, e.g., a Ramsey fringe experiment, in which the magnetic field strength is imprinted in the phase of the superpositioned state, is conducted, a large signal strength can be maintained without power broadening, thus a sensitivity up to $\sim 0.4\ \mu\mathrm{T}/\sqrt{\mathrm{Hz}}$, limited by the T_2^* of ∼1 μs, can be realized using a single NV center [2,19]. Further enhancement (below $1\ \mathrm{nT}/\sqrt{\mathrm{Hz}}$) is possible by using the NV center ensemble combined with the lock-in detection [20]. When the NV center is used for ac magnetic field sensing, spin echo type measurements can be used in which the long coherence time allows high sensitivity up to $\sim 1\ \mathrm{nT}/\sqrt{\mathrm{Hz}}$ using a single NV [22] and $\sim 0.9\ \mathrm{pT}/\sqrt{\mathrm{Hz}}$ using an NV ensemble [23].

Higher spin systems (S > 1) can also be used as a vector magnetometer in a similar way. For example, the silicon vacancy (V_{Si}) in silicon carbide (SiC) is known to possess a quartet manifold of $S = 3/2$ in its electronic ground state [24–26]. Because its ESR signal can be detected at ambient condition [4,11,27–29] even from a single defect [5] and the ZFS is in a range around a few millitesla depending on the polytype of SiC [3,4], its application as a dc magnetometer has been suggested [28,29]. Note that Simin *et al.* have recently shown an experimental application of V_{Si} in SiC as a submillitesla dc magnetometer based on approximated solutions for the spin Hamiltonian at weak magnetic fields [28].

In a spin system with a spin quantum number S, the strength and orientation of the applied magnetic field vector $\mathbf{B_0}$ determines the Zeeman splitting, thus one should experimentally obtain the Zeeman splitting to get information about $\mathbf{B_0}$. For $S = 1/2$, the Zeeman splitting is calculated from an observed single resonant transition energy $h\nu = g\mu_B B_0$, where g is the Landé g-factor, μ_B is the Bohr magneton, and h is Planck's constant. The information for the orientation can be extracted only if g is anisotropic. In high-spin systems, the orientation-related terms remain in the eigenvalue equation, which results in the orientation dependent shift of ESR spectra, which cannot be explained by $g\mu_B B_0$. It is, therefore, mandatory to reconstruct the energy eigenstates using the observed resonant energies. Because there exist $2S + 1$ eigenstates, $2S$ resonant transition energies should be experimentally determined. For example, when the applied magnetic field strength is much larger than the ZFS, i.e., $g\mu_B|\mathbf{B_0}| \gg$ ZFS, at least two transition energies should be known for $S = 1$ while three values are necessary for $S = 3/2$ as explained in Fig. 1. In this high-field range, the two transitions for $S = 1$ and two out of the three transitions for $S = 3/2$ cross each other as shown in Figs. 1(c) and 1(d). This leads to ambiguity in determining which observed ESR peak corresponds to which transition energy experimentally. In this report, we discuss

*s.lee@physik.uni-stuttgart.de

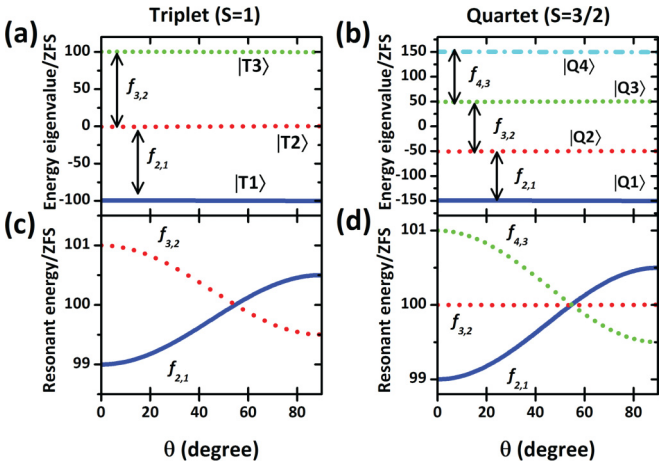

FIG. 1. (Color online) Energy eigenvalues and ESR transition energies of high-spin systems as a function of orientation at a high magnetic field $g\mu_B B_0 = 100 \times$ ZFS. (a) and (b) are the eigenvalues of the spin triplet ($S = 1$) and quartet ($S = 3/2$) states calculated numerically from Eq. (1), respectively. For numerical calculation, $D, E > 0$ and a uniaxial symmetry $E \ll D$ are assumed, thus, only the polar angle θ dependence is shown. Eigenstates are labeled in ascending order of corresponding energy eigenvalues. The most dominant transitions are indicated by the solid arrows with labels $f_{i,j}$ indicating a transition between |i⟩ and |j⟩. They are shown in (c) and (d) for the spin triplet and quartet states, respectively. All the energy values are normalized by ZFS.

how this ambiguity can be removed and thus show how to use the $S = 3/2$ system for vector magnetometry. For this, we will provide analytical solutions for the given $\mathbf{B_0}$ vector as a function of the resonant transition energies. We will present V_{Si} spins in SiC as a model system and also a novel magnetometry scheme using the magic angle. The discussion in this report is also applicable to other $S = 3/2$ systems, which have been found in fullerene [30–34], organic molecules [35–37], Ni impurities in diamond [38], and calcium oxide crystals [39].

II. VECTOR MAGNETOMETRY BASED ON $S = 3/2$ SPINS

In order to derive formulas for $B_0 \equiv |\mathbf{B_0}|$ and its orientation expressed by only three transition energies for $S = 3/2$, we will first construct the electronic spin Hamiltonian consisting of the ZFS and Zeeman term. The ZFS in high-spin systems can be described by the dipole-dipole interaction term in the spin Hamiltonian, $\mathbf{S} \cdot \mathbf{D} \cdot \mathbf{S}$, where $\mathbf{D}$ is the dipole-dipole coupling tensor. For simplicity, we assume an isotropic Landé g factor. Therefore, in the principal axis system of $\mathbf{D}$, in which the z axis is set to the symmetry axis, the electronic spin Hamiltonian at $\mathbf{B_0}$ is

$$H = g\mu_B \mathbf{B_0} \cdot \mathbf{S} + D\left[S_z^2 - S(S+1)/3\right] + E(S_+^2 + S_-^2)/2, \tag{1}$$

where E and D are the ZFS parameters, assumed to be positive, and $E \ll D$ if an uniaxial symmetry exists. For $S = 3/2$, the eigenvalue equation from Eq. (1) is, in the polar coordinate system,

$$\lambda^4 - \left(2D^2 + 6E^2 + \tfrac{5}{2}\beta_0^2\right)\lambda^2 - 2\beta_0^2[D(3\cos^2\theta - 1) + 3E\sin^2\theta\cos 2\phi]\lambda + \tfrac{9}{16}\beta_0^4 + D^4 - \tfrac{1}{2}D^2\beta_0^2 - D^2\beta_0^2(3\cos^2\theta - 1)$$
$$+ 3E^2(3E^2 + 2D^2) + E\beta_0^2\left(6D\sin^2\theta\cos 2\phi + \tfrac{9}{2}E\cos 2\theta\right) = 0, \tag{2}$$

where $\beta_0 \equiv g\mu_B B_0$. The numerically calculated eigenvalues at various orientations are shown in Fig. 2. When $\mathbf{B_0}$ is either parallel or perpendicular to the symmetry axis, the closed form solutions for each eigenvalue can be found as [16]

$$\lambda = \tfrac{1}{2}\beta_0 \pm \sqrt{(D+\beta_0)^2 + 3E^2} \quad \text{or} \quad -\tfrac{1}{2}\beta_0 \pm \sqrt{(D-\beta_0)^2 + 3E^2} \quad \text{for} \quad \mathbf{B_0} \| z \text{ axis},$$
$$\lambda = \tfrac{1}{2}\beta_0 \pm \sqrt{\beta_0^2 + D^2 + 3E^2 - (D-3E)\beta_0} \quad \text{or} \quad -\tfrac{1}{2}\beta_0 \pm \sqrt{\beta_0^2 + D^2 + 3E^2 + (D-3E)\beta_0} \quad \text{for} \quad \mathbf{B_0} \| x \text{ axis}, \tag{3}$$

which gives the eigenvalues at zero magnetic field, $\lambda_{B_0=0} = \pm \text{ZFS}/2$, where $\text{ZFS} \equiv 2\sqrt{D^2 + 3E^2}$. The eigenvalue equation for the general case can be expressed as

$$\sum_{n=0}^{2S+1} C_n \lambda^n = 0. \tag{4}$$

By plugging each eigenvalue λ_i into Eq. (4), one can obtain $2S + 1$ equations. The basic idea in order to find formulas for the $\mathbf{B_0}$ vector expressed by the observed resonant energies, is to remove all λ_i terms using the transition energy $f_{i,i-1} \equiv \lambda_i - \lambda_{i-1}$. Note that the energy eigenstates are not necessarily sorted with respect to the corresponding energy values. In other word, the indices can be randomly assigned to the states. Here, however, we keep the relation $\lambda_i > \lambda_{i-1}$ for convenience. We follow this approach, which has been frequently used for $S = 1$ systems [17,40]. First, $(2S - 1)$ sets of three simultaneous equations are obtained by plugging $\lambda_i + f_{i+1,i}$, λ_i, and $\lambda_i - f_{i,i-1}$ ($i = 2, 3, \ldots, 2S$) into Eq. (4). In each set, calculating

$$\sum_{n=0}^{2S+1} \frac{C_n\left[(\lambda_i + f_{i+1,i})^n - \lambda_i^n\right]}{C_{2S+1}} = 0 \quad \text{and}$$
$$\sum_{n=0}^{2S+1} \frac{C_n\left[(\lambda_i - f_{i,i-1})^n - \lambda_i^n\right]}{C_{2S+1}} = 0, \tag{5}$$

results in two new simultaneous equations:

$$\sum_{n=0}^{2S} C'_{i,n}\lambda_i^n = 0 \quad \text{and} \quad \sum_{n=0}^{2S} C''_{i,n}\lambda_i^n = 0. \tag{6}$$

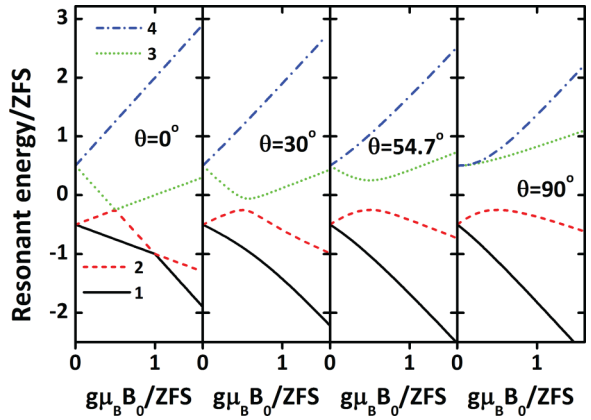

FIG. 2. (Color online) B_0 dependence of the energy eigenvalues of a spin quartet state at various magnetic field orientations. Eigenstates are labeled in ascending order of the corresponding energy eigenvalues. As $B_0 \to \infty$ at $\theta = 0^\circ$, $|4\rangle \to |m_S = +3/2\rangle$, $|3\rangle \to |m_S = +1/2\rangle$, $|2\rangle \to |m_S = -1/2\rangle$, and $|1\rangle \to |m_S = -3/2\rangle$.

Again, by taking the difference of the above terms divided by the coefficient of the highest-order term of each equation, respectively,

$$\sum_{n=0}^{2S} \frac{C'_{i,n}\lambda_i^n}{C'_{i,2S}} - \frac{C''_{i,n}\lambda_i^n}{C''_{i,2S}} = 0, \tag{7}$$

we obtain a new equation for the eigenvalue of the energy eigenstate $|i\rangle$ in which the highest power is $(2S-1)$,

$$\sum_{n=0}^{2S-1} C_{i,n}^{(2S-1)}\lambda_i^n = 0, \tag{8}$$

where $i = 2,3,\ldots,2S$. By repeating this procedure until only one linear equation for a single eigenvalue remains, one can find a formula for an eigenvalue expressed in terms of resonant energies, which allows us to find expressions for all other eigenvalues again using $f_{i,i-1}$. We use this procedure to find solutions for $S = 3/2$.

Following the procedure explained above, we obtain two equations for two energy eigenvalues, λ_2 and λ_3, expressed by only $f_{2,1}$ and $f_{3,2}$, and $f_{3,2}$ and $f_{4,3}$, respectively, and B_0, θ, and ϕ, which are present in both equations. Then using $f_{3,2} \equiv \lambda_3 - \lambda_2$ once again, we obtain formulas for each eigenvalue expressed by only the resonant energies as below

$$\begin{aligned}
\lambda_1 &= -\tfrac{3}{4}f_{2,1} - \tfrac{1}{2}f_{3,2} - \tfrac{1}{4}f_{4,3},\\
\lambda_2 &= \tfrac{1}{4}f_{2,1} - \tfrac{1}{2}f_{3,2} - \tfrac{1}{4}f_{4,3},\\
\lambda_3 &= \tfrac{1}{4}f_{2,1} + \tfrac{1}{2}f_{3,2} - \tfrac{1}{4}f_{4,3},\\
\lambda_4 &= \tfrac{1}{4}f_{2,1} + \tfrac{1}{2}f_{3,2} + \tfrac{3}{4}f_{4,3}.
\end{aligned} \tag{9}$$

By plugging one of these, e.g., λ_2, back into one of the equations found in the preceding steps, we finally obtain formulas for β_0^2, and a new quantity related to θ and ϕ, $\eta \equiv E(2\cos^2\phi\sin^2\theta + \cos^2\theta) + D\cos^2\theta$,

$$\beta_0^2 = \frac{\left(\frac{\sqrt{3}}{2}f_{4,3} + f_{3,2} + \frac{\sqrt{3}}{2}f_{2,1}\right)^2 + (1-\sqrt{3})(f_{4,3}+f_{2,1})f_{3,2} - f_{4,3}f_{2,1} - \mathrm{ZFS}^2}{5}, \tag{10}$$

$$\eta = \frac{4[8(D+3E) + 5(f_{4,3}-f_{2,1})]\beta_0^2 + (f_{4,3}-f_{2,1})\left[4\mathrm{ZFS}^2 - (f_{4,3}-f_{2,1})^2 - 4f_{3,2}^2\right]}{96\beta_0^2}. \tag{11}$$

Thus, in general, if D and E values are known and three resonant energies are observable, the applied magnetic field strength can be extracted from Eq. (10). In addition, if an uniaxial symmetry exists ($E \ll D$), because of $\eta \simeq D\cos^2\theta$, the polar angle can also be extracted from Eq. (11).

However, when one wants to use these formulas to find the external magnetic field vector, one may face a problem: how can one determine which observed resonant energy is from which transition? This is explained in Figs. 1 and 3. At a given magnetic field vector (e.g., $g\mu B_0 \gg$ ZFS), there will appear three strong transitions for $S = 3/2$ as in Fig. 3(a). The resonant energies are varying depending on the orientation for fixed B_0 and some of them even cross each other, thus it is hard to determine $f_{i,j}$ explicitly only taking into account these three transitions. However, in certain spin systems bound to certain localized defects in solids and at a certain magnetic field range, this ambiguity can be relaxed as will be shown in the following sections. We will focus on two distinguishable cases for $g\mu_B B_0 \ll$ ZFS and $g\mu_B B_0 \gg$ ZFS. The case for $g\mu_B B_0 \sim$ ZFS, however, will not be discussed because complex spectra appear due to a strong interaction among each eigenstate [21] via, e.g., the level anticrossing as in the NV centers [41], thus, high-spin systems are not an appropriate sensor for this field range. In the following sections, we will consider the uniaxial symmetry for all the numerical simulations unless noticed. This will allow us to utilize Eq. (11) to extract at least one orientation component θ.

A. High field, $g\mu_B B_0 \gg$ ZFS

Figure 3(a) depicts how each transition evolves at varying orientation θ at high static magnetic fields ($g\mu_B B_0 = 100 \times$ ZFS) together with ESR transition probabilities. $\mathbf{B_1}$ is assumed to have only an x-axis component. At high fields, three transitions are visible. Without knowing the information about B_0, it is not possible to assign them correctly because, as will be seen later, there appear also three or even more than three resonances that originate from different transitions at low magnetic fields. However, one can guess B_0 roughly from the observed resonant energies because they are approximately proportional to B_0 at high field. For example, $f_{3,2}$ shows very

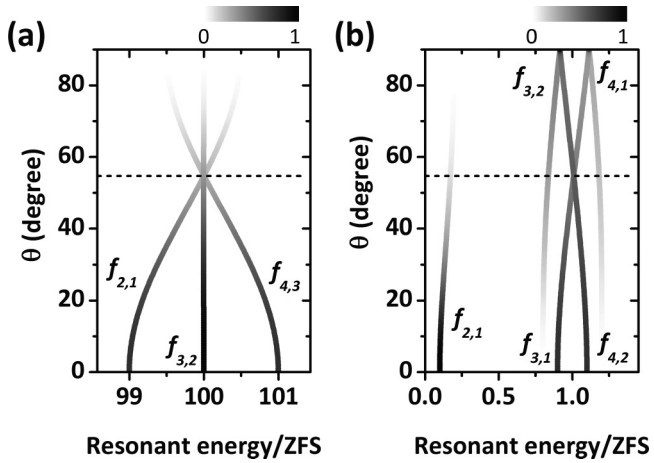

FIG. 3. Orientation dependence of ESR transitions at (a) high ($g\mu_B B_0 = 100 \times$ ZFS) and (b) low ($g\mu_B B_0 =$ ZFS/10) magnetic field strength. The dashed lines indicate the magic angle θ_m. The gray color scale depicts the normalized ESR transition probabilities for $\mathbf{B_1} \| x$ axis.

weak orientation dependence thus can be used to estimate B_0. Once the B_0 scale is roughly guessed, one can try to assign the observed resonant energies. Because $f_{3,2}$ always stays in the middle of all resonance transitions, this can be explicitly determined. And because Eq. (10) is invariant under switching of $f_{4,3}$ and $f_{2,1}$, B_0 can be unambiguously extracted. In contrast, Eq. (11) will result in a systematic error if $f_{4,3}$ and $f_{2,1}$ are not correctly assigned. Thus a magnetometer based on a $S = 3/2$ system can be used only to extract B_0 at a high magnetic field. This is a disadvantage compared to $S = 1$ because a similar equation to Eq. (11) is also invariant under switching of two observed resonant energies [17]. This problem, however, may be overcome by manipulating the ZFS [42]. If the electric dipole moment is large enough and their contribution to the ZFS Hamiltonian, the Stark-effect, is well-known, manipulation of the ZFS by either applying an electric field [42] or pressure [43] along a favored direction can result in shifts of each ESR transitions in different manners. Thus monitoring the additional shift upon the change in ZFS, may allow to determine all the necessary transitions and subsequently Eq. (11) can be used without systematic errors.

B. Low field, $g\mu_B B_0 \ll$ ZFS

Figure 3(b) shows that one can see up to five transitions at low field. At a small angle, there are three dominant transitions, $f_{2,1}$, $f_{3,1}$, and $f_{4,2}$, and two additional transitions, $f_{3,2}$ and $f_{4,1}$, which arise at large angle. Alternate forms of Eqs. (10) and (11) using only the most dominant transitions can be found for small angles (not shown). These forms, however, are not useful because $f_{4,2}$ and $f_{3,1}$ are changing their relative positions at a larger angle. Instead, $f_{4,1}$ and $f_{3,2}$ can be used since their relative positions are not changing and in certain $S = 3/2$ systems, e.g., V_{Si} in SiC (see Sec. III), these transitions show good intensities at every orientation [28]. The other useful formulas can be found by plugging $f_{4,3} = f_{4,1} - f_{3,2} - f_{2,1}$ into Eqs. (10) and (11) as

$$\beta_0^2 = \frac{(\sqrt{3} f_{\rm avg} + f_{2,1})^2 - 2 f_{4,1} f_{3,2} + (1-\sqrt{3}) f_{3,2} f_{2,1} - (1+\sqrt{3}) f_{41} f_{21} - {\rm ZFS}^2}{5}, \tag{12}$$

$$\eta = \frac{1}{96\beta_0^2}\{4[8(D+3E) + 5\Delta f_{\rm out} - 10 f_{2,1}]\beta_0^2 - 8 f_{2,1}({\rm ZFS}^2 - f_{2,1}^2 - f_{3,2}^2) + \Delta f_{\rm out}[4({\rm ZFS}^2 - 3 f_{2,1}^2 - f_{3,2}^2) + \Delta f_{\rm out}(6 f_{2,1} - \Delta f_{\rm out})]\}, \tag{13}$$

where $\Delta f_{\rm out} \equiv f_{4,1} - f_{3,2}$ and $f_{\rm avg} \equiv (f_{3,1} + f_{4,2})/2 = (f_{3,2} + f_{4,1})/2$. These are useful, because if $f_{4,1}$ and $f_{3,2}$ are observable together with $f_{4,2}$ and $f_{3,1}$, one always can unambiguously determine the two outermost transitions, and $f_{4,2}$ and $f_{3,1}$ are not in use or necessary only for calculating $f_{\rm avg}$.

So far, strategies to use $S = 3/2$ systems as a dc vector magnetometer have been discussed in both high- and low-magnetic field ranges. Though only B_0 can be obtained at high fields using only a conventional experimental method, both B_0 and polar angle can be determined at low field. However, in many high-spin systems bound to localized defects in solids, spin-dependent intersystem crossing may induce a strong polarization into specific spin states as in V_{Si} in SiC [10,25]. Thus, some transitions may be hardly observable. In addition, because only the polar angle can be obtained, it is still not possible to realize a genuine vector magnetometry. In the following sections, we will present $S = 3/2$ spins of V_{Si} in SiC as a model system and discuss the practical usage of them and a possible way to use them as a vector magnetometer.

III. SILICON VACANCY SPINS IN SILICON CARBIDE AS A DC VECTOR MAGNETOMETER

We present V_{Si} in SiC as a model system to provide explanations about how the formulas, found in previous sections, can be used to experimentally reconstruct the applied external magnetic field vector. Because spin properties are different depending on the polytype, here we discuss only a specific polytype, namely 4H-SiC. In addition, because there exist two inequivalent lattice sites, there appear two different silicon vacancies with different ZFS, and we choose only one of them known as T_{V2a} center [3,4]. In the T_{V2a} center, it is known that there exist an uniaxial symmetry around the c axis thus $E \ll D$ and ${\rm ZFS}/h \simeq 2D/h \simeq 70$ MHz [3,4]. It is also known that optical polarization results in equal

populations in two substates, $|m_S = \pm 1/2\rangle$. This is responsible for the absence of a transition between $|m_S = +1/2\rangle$ and $|m_S = -1/2\rangle$ while another two transitions, between $|m_S = +3/2\rangle$ and $|m_S = +1/2\rangle$ and between $|m_S = -3/2\rangle$ and $|m_S = -1/2\rangle$, are observable in the ESR spectra of T_{V2a} for $\mathbf{B_0} \| c$ axis [3,5,9–11,27–29]. In the $\mathbf{B_0}$ orientation dependence at low [28] and high magnetic fields [3,10,27,29], one of the allowed transitions, corresponding to the transition between $|m_S = +1/2\rangle$ and $|m_S = -1/2\rangle$ for $\mathbf{B_0} \| c$ axis, has not been observed probably due to that this equal population is somehow maintained. This will prevent Eqs. (10)–(13) from being used because $f_{3,2}$ at high fields and $f_{2,1}$ at low fields will not be observable. This transition, however, can become visible once electron-electron double resonance (ELDOR) is applied. The population difference between $|m_S = \pm 1/2\rangle$ states can be induced by applying, e.g., a resonant π pulse between $|m_S = +3/2\rangle$ and $|m_S = +1/2\rangle$ (or $|m_S = -1/2\rangle$ and $|m_S = -3/2\rangle$) states, which enable detection of this missing transition [25]. This will allow unambiguous determination of one transition $f_{2,1}$ at low fields or $f_{3,2}$ at high fields experimentally.

At high magnetic field (e.g., $B_0 \sim 300$ mT) as in Fig. 3(a), two outer transitions, $f_{4,3}$ and $f_{2,1}$ have been observed experimentally at almost all orientations at both cryogenic [3,10] and room temperature [29] except the central peak. The central peak is observable by ELDOR experiments [25], thus Eq. (10) can be used as explained in Sec II A. However, the polar angle, θ, can be determined from Eq. (11) only at small angles because of the ambiguity on determining $f_{4,3}$ and $f_{2,1}$ at larger angles.

ESR spectra of T_{V2a} centers at a low magnetic field (e.g., submillitesla), as in Fig. 3(b), allow an unambiguous determination of both B_0 and polar angle as long as the ELDOR can be used to determine $f_{2,1}$ as explained in Sec. II B. However, one can consider another case in which either ELDOR experiments are not available or $f_{2,1}$ is hardly observed in the ELDOR spectrum. In such a case, if $f_{4,1}$ and $f_{3,2}$ are observable, using relations $f_{3,1} + f_{4,2} = f_{3,2} + f_{4,1}$, $f_{4,3} = f_{4,2} - f_{3,2}$, and $f_{2,1} = f_{3,1} - f_{3,2}$ from Eq. (9), we again obtain alternative forms of Eqs. (10) and (11) as

$$B_0^2 = \frac{(\sqrt{3} f_{\rm avg} + f_{3,2})^2 - f_{4,2} f_{3,1} - 2(\sqrt{3}+1) f_{3,2} f_{\rm avg} - {\rm ZFS}^2}{5}, \tag{14}$$

$$\eta = \frac{[32(D+3E) + 20\Delta f_{\rm in}] B_0^2 + \Delta f_{\rm in}\left(4{\rm ZFS}^2 - \Delta f_i^2 - 4 f_{3,2}^2\right)}{96 B_0^2}, \tag{15}$$

where $\Delta f_{\rm in} \equiv f_{4,2} - f_{3,1}$. Note that $f_{3,2}$ appears in both formulas but because it is always the lowest energy transition, this can be explicitly determined. Similarly, one can find additional alternatives using $f_{4,1}$ instead of $f_{3,2}$. Therefore, even if ELDOR is not available, as long as either $f_{4,1}$ or $f_{3,2}$ is observable together with $f_{4,2}$ and $f_{3,1}$, B_0 can be extracted using Eq. (14) because it is invariant under switching $f_{4,2}$ and $f_{3,1}$. This scheme is feasible since $f_{4,1}$ and $f_{3,2}$ are observable from T_{V2a} in SiC by cw methods with a decent signal strength at sub-milli-tesla as recently reported [28]. Equation (15), however, still cannot provide an unambiguous way to determine the polar angle because of $\Delta f_{\rm in}$, which changes signs if $f_{4,2}$ and $f_{3,1}$ are not correctly determined.

So far, the strategies to use $V_{\rm Si}$ in SiC as a vector magnetometer has been discussed. While the magnetic field strength can be extracted in both high and low magnetic field ranges, the orientation can be extracted only if there exists a uniaxial symmetry at a low magnetic field, and the azimuthal angle cannot be determined in any case. Note that the $S = 1$ system with the uniaxial symmetry also can provide only the polar angle. But in the case of the NV center in diamond, because the NV centers can be in four different orientations along the diamond bond axes, one can determine both the polar and azimuthal angles from the shift of transitions of the inequivalently oriented NV centers. Similarly, $V_{\rm Si}$ in inequivalent lattice sites, e.g., T_{V1a} and T_{V2a} in 4H-SiC, and T_{V1a}, T_{V2a}, and T_{V3a} in 6H-SiC [4] can also be utilized. However, ESR spectra of T_{V1a} and T_{V3a} are hardly visible at room temperature [4,9,27]. Thus, an alternate method relying only on the T_{V2a} center that can be used for any magnetic field strength at room temperature is necessary. In the next section, another method using a magic angle that allows for the use of $S = 3/2$ as a vector magnetometer will be discussed.

IV. VECTOR MAGNETOMETRY USING MAGIC ANGLE

We start from the eigenvalue equation (2). In this equation, one can find terms including $(3\cos^2\theta - 1)$, which becomes zero at the magic angle $\theta_m \simeq 54.7^\circ$. Equation (2) can be simplified for $\theta = \theta_m$ and $E \ll D$ as

$$\lambda^4 - \left(2D^2 + \tfrac{5}{2}\beta_0^2\right)\lambda^2 + \tfrac{9}{16}\beta_0^4 + D^4 - \tfrac{1}{2}D^2\beta_0^2 = 0, \tag{16}$$

and the eigenvalues are simply

$$\lambda = \pm\tfrac{1}{2}\sqrt{4D^2 + 5\beta_0^2 \pm 4\sqrt{3\beta_0^2 D_0^2 + \beta_0^4}}, \tag{17}$$

as depicted in Fig. 2(c). For high B_0, these can be again approximated as

$$\lambda = \pm\tfrac{3}{2}\beta_0 \quad \text{or} \quad \pm\tfrac{1}{2}\beta_0 \quad (\text{for } g\mu_B B_0 \gg {\rm ZFS}). \tag{18}$$

Thus, at θ_m, we obtain $|\lambda_1| = |\lambda_4|$ and $|\lambda_2| = |\lambda_3|$, and can see the least number of transitions as seen in Fig. 3. We can use this aspect to use $S = 3/2$ system as a vector magnetometer. If the spin sensor is being rotated around an axis and the orientation between the c axis and the rotational axis is fixed to θ_m, one expects to see the least number of transitions whose widths are the narrowest when the rotational axis is aligned to the applied external magnetic field. In contrast, when the rotational axis is misaligned, very broad ESR transitions appear due to orientation sweeping.

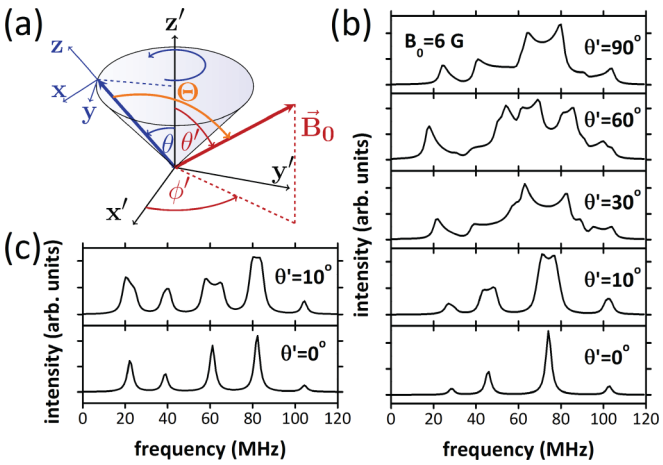

FIG. 4. (Color online) Magic angle dc magnetometry based on a $S = 3/2$ spin system. (a) describes the frames used for the numerical simulation. See text for details. (b) shows the numerical simulations of the cw ESR spectra when the $S = 3/2$ spin is misaligned by $\theta = \theta_m$ relative to the rotational axis at various orientations of $\mathbf{B_0}$ vector in y'-z' plane at low field $B_0 = 6\,G$. For the simulation, the ZFS of T_{V2a} center in SiC, $\mathrm{ZFS}/h \simeq 2D/h \simeq 70$ MHz is assumed. (c) shows the same simulation but for the case when $\theta \neq \theta_m$ and $\theta = 30^\circ$.

Figure 4 describes such an experiment in which the SiC crystal is attached to a rotational axis forming θ_m with respect to the c axis of the crystal. The resonant RF can be applied using a miniature coil surrounding either the rotational axis or the SiC crystal, similar to what has been suggested for the quantum gyroscope based on the NV center [44]. For the detection, a small sized ESR cavity can be used for conventional ESR detection. Fiber coupling also can be considered for ODMR. If an electrically detected magnetic resonance is possible, which has recently been shown in high-spin systems [45] and also in SiC [46], additional small circuits can be utilized. B_1 field modulation can be used to enhance the signal to noise ratio [47] because the ELDOR experiment, which requires B_1 pulses, is not necessary for this experiment. For the simulation of ESR spectra in this experiment, a laboratory frame is assumed: the z' axis is set to the rotational axis. The angle Θ between the c axis of the crystal, rotating with a constant speed around the z' axis, and the external magnetic field can be derived and replace θ in Eq. (2). For convenience, the RF field is assumed to be in the x axis of the rotating frame. By assuming a Lorentzian lineshape with 3 MHz FWHM, the numerically simulated ESR spectra at varying θ' while ϕ' is fixed to 90° are simulated for a low field ($B_0 = 6G$) as shown in Fig. 4(b). As expected, when $\theta' = 0$, equivalently, $\Theta = \theta_m$ or $\mathbf{B_0} \| z' -$ axis, the narrowest transitions are found, while seriously broadened peaks like a powder pattern appear when misaligned ($\theta' \neq 0$). Note that in order to present a general $S = 3/2$ case, $f_{2,1}$ is assumed to be visible in cw ESR spectra at low field. Therefore by monitoring the linewidth of the observed transition spectra, while moving the rotational axis, z' axis, one can explicitly find the orientation of the external magnetic field. The field strength also can be extracted from the observed resonant energy of the strongest transition using Eq. (17). For very small field $g\mu_B B_0 \ll \mathrm{ZFS}$, $f_{3,1} = f_{4,2} \approx g\mu_B B_0 + 4g\mu_B B_0 D^2/3$. We also can observe spectra consisting of the narrow transitions even if $\theta \neq \theta_m$ as long as $\theta' = 0$. However, because many transitions whose intensities are comparable to each other appear as in Fig. 4(c), it is more convenient to use the magic angle because the most dominant transition is easily distinguishable.

V. CONCLUSION

We have shown that using the V_{Si} in SiC as a model system, $S = 3/2$ electronic spins with the uniaxial symmetry can be used to find the strength and polar angle of the applied external magnetic field if at least three ESR transitions can be found experimentally and the ZFS parameters are known. At a high B_0 field ($g\mu_B B_0 \gg \mathrm{ZFS}$), B_0 can be obtained from the observed ESR spectra but the polar angle cannot be determined due to the ambiguity of differentiating two outer transitions. In contrast, at low $g\mu_B B_0$ ($\ll$ZFS), as long as one can explicitly identify at least three transitions including the allowed lowest energy transition, the external magnetic field vector can be reconstructed. In a field strength comparable to the ZFS, it is hard to find a useful scheme because very complex patterns appear due to mixing of some of the eigenstates. In the case of the NV centers in diamond ($\mathrm{ZFS}/h = 2.87$ GHz), this missing range is around $\sim$100 mT. The V_{Si} in SiC can fill out this gap since its ZFS is quite small ($\mathrm{ZFS}/h \sim 100$ MHz) thus this magnetic field range can be considered as a high-field range in which the three necessary transitions are well observable [25,29], and at least the field strength can be experimentally determined. When the V_{Si} in SiC is used to realize such schemes at submillitesla, if the lowest transition energy is observable by ELDOR, one can determine both B_0 and θ without ambiguity. Even if ELDOR is not available, thanks to the additional transitions that appear at low fields, the field strength can be determined.

The magic angle terms in the eigenvalue equation allow for an alternative method to use $S = 3/2$ systems as a dc vector magnetometer. If the $S = 3/2$ spins fixed in a crystal can be rotated around the rotational axis, the unambiguous determination of the applied magnetic field vector is feasible by monitoring the linewidth of the observed ESR spectra while the symmetry axis of the crystal is oriented at θ_m relative to the rotational axis and the rotational axis is moving. This configuration also can be realized by producing an array of crystals such that the symmetry axes of each crystal form a cone whose opening angle is twice the magic angle.

These findings provide a better understanding of the $S = 3/2$ electronic spin Hamiltonian, especially at low fields. They also provide an outlook for the application of V_{Si} in SiC to quantum magnetometry, which is promising thanks to the electrical properties of SiC, which outstand the host material of the NV centers, and the mature fabrication technology, which allows an efficient fabrication of electronic devices even at the atomic scale [48].

ACKNOWLEDGMENTS

We thank Torsten Rendler, Seoyoung Paik, Thomas Wolf, Matthias Widmann for helpful discussions, and Nathan Chejanovsky for helping to prepare this manuscript. We acknowledge funding by the DFG via priority programme 1601 and the EU via ERC Grant SQUTEC and Diadems as well as the Max Planck Society.

[1] M. W. Doherty, N. B. Manson, P. Delaney, F. Jelezko, J. Wrachtrup, and L. C. L. Hollenberg, Phys. Rep. **528**, 1 (2013).

[2] R. Schirhagl, K. Chang, M. Loretz, and C. L. Degen, Ann. Rev. Phys. Chem. **65**, 83 (2014).

[3] E. Sörman, N. T. Son, W. M. Chen, O. Kordina, C. Hallin, and E. Janzén, Phys. Rev. B **61**, 2613 (2000).

[4] E. Janzén, A. Gali, P. Carlsson, A. Gällström, B. Magnusson, and N. T. Son, Physica B: Condens. Matter **404**, 4354 (2009).

[5] M. Widmann, S.-Y. Lee, T. Rendler, N. T. Son, H. Fedder, S. Paik, L.-P. Yang, N. Zhao, S. Yang, I. Booker, A. Denisenko, M. Jamali, S. A. Momenzadeh, I. Gerhardt, T. Ohshima, A. Gali, E. Janzén, and J. Wrachtrup, Nat. Mater. **14**, 164 (2015).

[6] D. J. Christle, A. L. Falk, P. Andrich, P. V. Klimov, J. U. Hassan, N. T. Son, E. Janzén, T. Ohshima, and D. D. Awschalom, Nat. Mater. **14**, 160 (2015).

[7] J. R. Weber, W. F. Koehl, J. B. Varley, A. Janotti, B. B. Buckley, C. G. Van de Walle, and D. D. Awschalom, Proc. Natl. Acad. Sci. USA **107**, 8513 (2010).

[8] W. F. Koehl, B. B. Buckley, F. J. Heremans, G. Calusine, and D. D. Awschalom, Nature (London) **479**, 84 (2011).

[9] P. G. Baranov, A. P. Bundakova, A. A. Soltamova, S. B. Orlinskii, I. V. Borovykh, R. Zondervan, R. Verberk, and J. Schmidt, Phys. Rev. B **83**, 125203 (2011).

[10] N. Mizuochi, S. Yamasaki, H. Takizawa, N. Morishita, T. Ohshima, H. Itoh, and J. Isoya, Phys. Rev. B **66**, 235202 (2002).

[11] H. Kraus, V. A. Soltamov, D. Riedel, S. Vath, F. Fuchs, A. Sperlich, P. G. Baranov, V. Dyakonov, and G. V. Astakhov, Nat. Phys. **10**, 157 (2014).

[12] K. Szász, V. Ivády, I. A. Abrikosov, E. Janzén, M. Bockstedte, and A. Gali, Phys. Rev. B **91**, 121201 (2015).

[13] A. Gali, A. Gällström, N. T. Son, and E. Janzén, Mater. Sci. Forum **645–648**, 395 (2010).

[14] N. T. Son, P. Carlsson, J. ul Hassan, E. Janzén, T. Umeda, J. Isoya, A. Gali, M. Bockstedte, N. Morishita, T. Ohshima, and H. Itoh, Phys. Rev. Lett. **96**, 055501 (2006).

[15] R. C. Stevenson, J. Magn. Reson. **57**, 24 (1984).

[16] N. M. Atherton, *Ellis Horwood Series in Physical Chemistry* (Ellis Horwood, Chichester, 1993).

[17] G. Balasubramanian, I. Y. Chan, R. Kolesov, M. Al-Hmoud, J. Tisler, C. Shin, C. Kim, A. Wojcik, P. R. Hemmer, A. Krueger, T. Hanke, A. Leitenstorfer, R. Bratschitsch, F. Jelezko, and J. Wrachtrup, Nature (London) **455**, 648 (2008).

[18] S. Steinert, F. Dolde, P. Neumann, A. Aird, B. Naydenov, G. Balasubramanian, F. Jelezko, and J. Wrachtrup, Rev. Sci. Instrum. **81**, 043705 (2010).

[19] J. M. Taylor, P. Cappellaro, L. Childress, L. Jiang, D. Budker, P. R. Hemmer, A. Yacoby, R. Walsworth, and M. D. Lukin, Nat. Phys. **4**, 810 (2008).

[20] H. Clevenson, M. E. Trusheim, C. Teale, T. Schroder, D. Braje, and D. Englund, Nat. Phys. **11**, 393 (2015).

[21] C. L. Degen, Appl. Phys. Lett. **92**, 243111 (2008).

[22] G. Balasubramanian, P. Neumann, D. Twitchen, M. Markham, R. Kolesov, N. Mizuochi, J. Isoya, J. Achard, J. Beck, J. Tissler, V. Jacques, P. R. Hemmer, F. Jelezko, and J. Wrachtrup, Nat. Mater. **8**, 383 (2009).

[23] T. Wolf, P. Neumann, K. Nakamura, H. Sumiya, J. Isoya, and J. Wrachtrup, arXiv:1411.6553 [quant-ph].

[24] N. Mizuochi, S. Yamasaki, H. Takizawa, N. Morishita, T. Ohshima, H. Itoh, and J. Isoya, Phys. Rev. B **68**, 165206 (2003).

[25] J. Isoya, T. Umeda, N. Mizuochi, N. T. Son, E. Janzén, and T. Ohshima, Physica Status Solidi (b) **245**, 1298 (2008).

[26] N. Mizuochi, S. Yamasaki, H. Takizawa, N. Morishita, T. Ohshima, H. Itoh, T. Umeda, and J. Isoya, Phys. Rev. B **72**, 235208 (2005).

[27] V. A. Soltamov, A. A. Soltamova, P. G. Baranov, and I. I. Proskuryakov, Phys. Rev. Lett. **108**, 226402 (2012).

[28] D. Simin, F. Fuchs, H. Kraus, A. Sperlich, P. G. Baranov, G. V. Astakhov, and V. Dyakonov, Phys. Rev. Appl. **4**, 14009 (2015).

[29] H. Kraus, V. A. Soltamov, F. Fuchs, D. Simin, A. Sperlich, P. G. Baranov, G. V. Astakhov, and V. Dyakonov, Sci. Rep. **4**, 5303 (2014).

[30] J. J. L. Morton, A. M. Tyryshkin, A. Ardavan, K. Porfyrakis, S. A. Lyon, and G. A. D. Briggs, J. Chem. Phys. **122**, 174504 (2005).

[31] C. Knapp, N. Weiden, H. Kass, K.-P. Dinse, B. Pietzak, M. Waiblinger, and A. Weidinger, Mol. Phys. **95**, 999 (1998).

[32] W. Harneit, Phys. Rev. A **65**, 032322 (2002).

[33] S. C. Benjamin, A. Ardavan, G. A. D. Briggs, D. A. Britz, D. Gunlycke, J. Jefferson, M. A. G. Jones, D. F. Leigh, B. W. Lovett, and A. N. Khlobystov, J. Phys.: Condens. Matter **18**, S867 (2006).

[34] N. Mizuochi, Y. Ohba, and S. Yamauchi, J. Chem. Phys. **111**, 3479 (1999).

[35] Y. Teki, S. Miyamoto, M. Nakatsuji, and Y. Miura, J. Am. Chem. Soc. **123**, 294 (2001).

[36] G. Kothe, S. S. Kim, and S. I. Weissman, Chem. Phys. Lett. **71**, 445 (1980).

[37] Y. Teki, H. Tamekuni, K. Haruta, J. Takeuchi, and Y. Miura, J. Mater. Chem. **18**, 381 (2008).

[38] J. Isoya, H. Kanda, J. R. Norris, J. Tang, and M. K. Bowman, Phys. Rev. B **41**, 3905 (1990).

[39] P. A. van Leeuwen, R. Vreeker, and M. Glasbeek, Phys. Rev. B **34**, 3483 (1986).

[40] M. S. de Groot and J. H. van der Waals, Mol. Phys. **3**, 190 (1960).

[41] X.-F. He, N. B. Manson, and P. T. H. Fisk, Phys. Rev. B **47**, 8809 (1993).

[42] F. Dolde, H. Fedder, M. W. Doherty, T. Nobauer, F. Rempp, G. Balasubramanian, T. Wolf, F. Reinhard, L. C. L. Hollenberg, F. Jelezko, and J. Wrachtrup, Nat. Phys. **7**, 459 (2011).

[43] A. L. Falk, P. V. Klimov, B. B. Buckley, V. Ivády, I. A. Abrikosov, G. Calusine, W. F. Koehl, A. Gali, and D. D. Awschalom, Phys. Rev. Lett. **112**, 187601 (2014).

[44] A. Ajoy and P. Cappellaro, Phys. Rev. A **86**, 062104 (2012).

[45] E. Bourgeois, A. Jarmola, M. Gulka, J. Hruby, D. Budker, and M. Nesladek, arXiv:1502.07551 [cond-mat.mes-hall].

[46] C. J. Cochrane, P. M. Lenahan, and A. J. Lelis, Appl. Phys. Lett. **100**, 023509 (2012).

[47] S.-Y. Lee, S. Paik, D. R. McCamey, and C. Boehme, Phys. Rev. B **86**, 115204 (2012).

[48] A. Lohrmann, N. Iwamoto, Z. Bodrog, S. Castelletto, T. Ohshima, T. J. Karle, A. Gali, S. Prawer, J. C. McCallum, and B. C. Johnson, Nat. Commun. **6**, 7783 (2015).